# Berry phase and its sign in quantum superposition states of thermal $^{87}$Rb atoms

S. Welte, C. Basler, and H. Helm[*]

*Department of Molecular and Optical Physics, University of Freiburg, Stefan-Meier-Strasse 19, 79104 Freiburg, Germany*
(Received 28 November 2013; published 10 February 2014)

We investigate the Berry phase in an ensemble of thermal $^{87}$Rb atoms which we prepare in a superposition state under conditions near and at electromagnetically induced transparency. The geometric phase is imprinted in the atoms by rotating the laboratory magnetic field. Phase-stabilized light fields permit us to monitor phase changes of the atomic sample in a Ramsey-type interferometer by instant probing of the absorptive response of the atoms as well as by monitoring the free-induction decay of the coherent superposition. The absolute sign of the phase is determined by reference to controllable phase shifts imposed by the experimenter. We prove that the geometric phase is independent of the rotational frequency of the magnetic field in the adiabatic regime, that the phase is additive in multiple rotations, and it is independent of the Landé factor of the atomic magnetic moment, as predicted in Berry's seminal paper. We show that the absolute sign of the phase encodes the sign of the observable angular momentum in relation to laboratory coordinates.

## I. INTRODUCTION

The appearance of a geometric phase $\gamma$ in the wave function of a quantum system which follows a cyclic adiabatic evolution of its Hamiltonian along some trajectory $\mathcal{C}$ in parameter space was described by Berry in 1984 [1]. The circuit-dependent phase component $e^{i\gamma}$ which appears in addition to the familiar dynamic phase $e^{-iEt/\hbar}$ of any stationary state had been recognized earlier as the sign change in molecular systems which propagate around a degeneracy of the eigenstates [2,3] and as the sign change of spinors slowly rotated by $2\pi$ [4]. Additional experimental verification followed in transport of light through an optical fiber around a closed loop in momentum space [5] and by neutron spin rotation in adiabatic transport of neutrons through a helical magnetic field [6]. Tycko imprinted the geometric phase on a nuclear spin by mechanic rotation of a crystal in a magnetic field [7]. The effect on a superposition state of cold atoms in a MOT was studied in an atom interferometer [8] using external parameters such as laser phase and laser polarization. Of interest in quantum information experiments is that phases can be insensitive to parameter noise, a feature discussed in Refs. [9,10]. Recently, Morinaga and coworkers explored the Berry phase in a cloud of cold sodium atoms and invoked an effect of the *sign* of the Landé factor on the phase [11–13]. Such a dependence had previously been referred to by Richardson [14]. The dimensionless Landé factor $g_F$ characterizes the observable magnetic moment of an atomic state in units of the Bohr magneton $\mu_B$ and the energy of a Zeeman state with magnetic quantum number $m_F$ at low field strength,

$$E = -m_F \, g_F \, \mu_B B. \tag{1}$$

An effect of the actual magnetic moment associated with the angular momentum vector on the geometric phase is not predicted in Berry's work [1] or in later discussions of this subject [15], and appears out of line with the purely geometric effect of rotation of a state vector.

Here, we report a study of Berry's phase in an ensemble of thermal $^{87}$Rb atoms. The geometric phase is imprinted in the relative phase of superposition states of two hyperfine components in controlled rotations of the laboratory magnetic field. Two methods are used to pin down the sign of this phase. One relies on imprinting a controllable additional phase shift of known sign, either by the ac Stark effect or by a small detuning of the laser fields. Here the sign of the geometric phase can be inferred from the compensation point where both phases balance, resulting in a total phase shift of zero. A second method detects the sign from the phase of the oscillatory free-induction decay, which occurs when exposing the superposition state to nonresonant light fields. The magnitude of the Berry phase obtained by these methods is shown to agree with results of measurements where no external or dynamic phase shifts are introduced. We show that the observable phase of a superposition state advances with a geometric phase proportional to the difference of magnetic quantum numbers of the state and the signed solid angle of the magnetic field circuit, independent of the sign of the Landé factor.

## II. BERRY PHASE

When rotating a laboratory magnetic field an atomic wavefunction acquires a geometric phase depending on the geometry of the path encircled by the magnetic field vector $\vec{B}$. Berry showed that the geometric phase $\gamma$ imprinted on a state $|\psi\rangle$ is

$$\gamma = i \oint_{\mathcal{C}} \langle \psi(\vec{B})|\vec{\nabla}_{\vec{B}}|\psi(\vec{B})\rangle \, d\vec{B} \tag{2}$$

$$= -\iint_{S(C)} \vec{V}_\psi(\vec{B}) d\vec{S}. \tag{3}$$

The integrand in Eq. (2) is referred to as the Berry connection and can be viewed as a gauge or vector potential. The field

———————
[*]helm@uni-freiburg.de
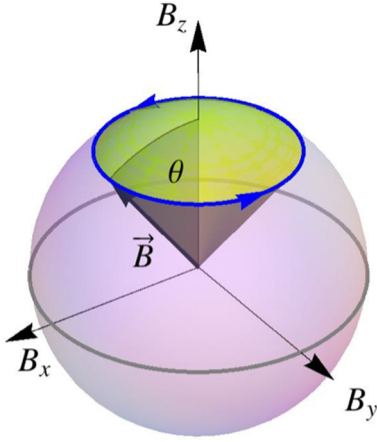
FIG. 1. (Color online) Rotation of the magnetic field vector around the $z$ axis. Initially, $\vec{B}$ points along the positive $z$ direction. It is then tilted by an angle $\theta$. Under this angle of latitude the vector is rotated once around the $z$ axis before being aligned into the $z$ direction again. The direction of rotation indicated by the blue arrows refers to a positive sign of the signed cone angle $\theta$.

strength (curvature form) is

$$\vec{V}_\psi(\vec{B})$$

$$= \mathrm{Im} \sum_{\psi \neq \psi'} \frac{\langle \psi(\vec{B})|\vec{\nabla}_{\vec{B}}\mathcal{H}(\vec{B})|\psi'(\vec{B})\rangle \times \langle \psi'(\vec{B})|\vec{\nabla}_{\vec{B}}\mathcal{H}(\vec{B})|\psi(\vec{B})\rangle}{[E_{\psi'}(\vec{B}) - E_\psi(\vec{B})]^2}.$$

(4)

where $\mathcal{H}(\vec{B})$ is the Hamiltonian of the interaction with the magnetic field $\vec{B}$. If the time taken by the magnetic field vector to follow the closed path $\mathcal{C}$ is much longer than the inverse Larmor precession frequency of the total angular momentum, the dynamics is said to be adiabatic. In this case the geometric phase is independent of the speed at which we move the magnetic field vector.[1] When the Landé factor appears linearly in the gradient $\vec{\nabla}_{\vec{B}}\mathcal{H}$, such as the first-order perturbation result (1), one can readily show [15] that the Berry phase is independent of the sign and magnitude of $g_F$ since it occurs quadratically in the numerator and denominator of Eq. (4). This emphasizes that the Berry phase is a geometric property associated with the angular momentum vector only, irrespective of the direction of the magnetic moment or its strength, albeit the latter is used in an experiment to transport the angular momentum vector.

For a Zeeman state with magnetic quantum number $m_F$ the geometric phase (2) simplifies in the adiabatic case to [1]

$$\gamma = -m_F \Omega(\mathcal{C}),$$

(5)

where $\Omega(\mathcal{C})$ is the solid angle subtended by the closed path $\mathcal{C}$ as seen from the origin $\vec{B} = 0$; that is, the solid angle spanned by the tip of the external magnetic field vector on $\mathcal{C}$. An example of a path $\mathcal{C}$ following a spherical surface is shown in Fig. 1. Here the magnetic field vector is first tilted from the laboratory
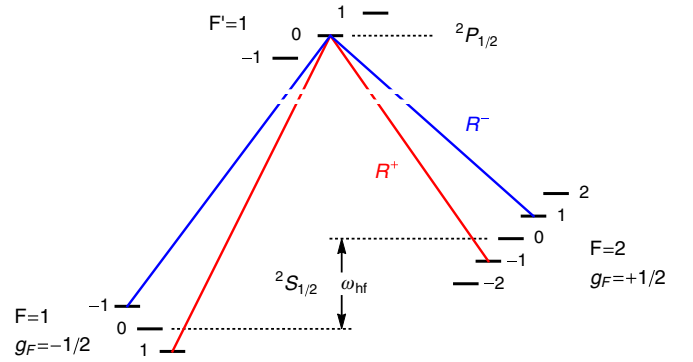


FIG. 2. (Color online) Two EIT resonances of $^{87}$Rb. The two ground states $F = 1$ and $F = 2$ have opposite sign of the Landé factor.

$z$ axis by an angle $\theta$. The $z$ axis serves to define the magnetic quantum numbers $m_F$ in the preparation stage of the quantum system. Then the magnetic field vector is rotated once along a cone with solid angle

$$\Omega(\mathcal{C}) = \mathrm{sgn}(\theta)2\pi(1 - \cos\theta).$$

(6)

The factor $\mathrm{sgn}(\theta)$ defines the orientation of the surface normal $\hat{n}$. For clockwise rotation around the $z$ axis (viewed in direction of the positive $z$ axis) the sign is taken positive according to the right-hand rule, determined by the sign of the scalar product of the magnetic field vector $\vec{B}$ and the normal vector $\hat{n}$ on the surface of motion.

## III. ATOMIC STATE AND PHASE DETECTION

Our phase sensitive quantum system are atoms in a superposition of two Zeeman levels of the ground states of $^{87}$Rb which are separated in energy by the hyperfine splitting $E_2 - E_1 = \omega_{\mathrm{hf}}$. The nonstationary superposition state $|\psi_{\mathrm{NC}}(t)\rangle$ is

$$|\psi_{\mathrm{NC}}(t)\rangle = (|1\rangle - e^{-i(\omega_{\mathrm{hf}}t + \phi_0)}|2\rangle)/\sqrt{2},$$

(7)

where $|1\rangle$ refers to a Zeeman level in $F = 1$ and $|2\rangle$ refers to a Zeeman level in $F = 2$. In (7) we suppressed the common phase factor $e^{-iE_1 t/\hbar}$. The superposition state (7) is prepared by two copropagating laser fields

$$\mathcal{E}_j = \mathcal{E}_j^0 \cos(\omega_j t + \phi_j - k_j z), \quad j = 1,2,$$

(8)

of opposite circular polarization. The laser frequencies and polarization may be chosen to realize one of the two $\Lambda$ schemes shown in Fig. 2, $R^+$ or $R^-$ or both when the lasers are parallel linearly polarized. For ease of writing Eq. (7) we assumed equal Rabi frequencies of the two lasers, $g_1 = g_2 = g$. The Hamiltonian describing the interaction with the light fields is

$$H_{\mathrm{int}} = \frac{g\,\hbar}{2}(e^{-i(\omega_1 t + \phi_1)}|1\rangle\langle 3| + e^{-i(\omega_2 t + \phi_2)}|2\rangle\langle 3| + \mathrm{H.c.}),$$

(9)

where we suppressed the spatial dependence of (8) and where $|3\rangle$ refers to the common excited level in Fig. 2, $F' = 1$, $m_{F'} = 0$.

When the frequency difference of the laser fields $\omega_2 - \omega_1$ matches the hyperfine splitting $\omega_{\mathrm{hf}}$ and when the laser phase difference matches the relative phase difference in the

---

[1]A generalization of the geometric phase to nonadiabatic evolution was given by Aharonov and Anandan [16].

superposition state $\phi_2 - \phi_1 = \phi_0$, the superposition state is nonabsorbing as we find

$$H_{\text{int}}|\psi_{\text{NC}}(t)\rangle = 0. \tag{10}$$

In other words if the laser fields are in two-photon resonance with the ground state energy difference and if the phase in the superposition state $\phi_0$ mirrors the phase difference in the two laser fields $\phi_2 - \phi_1$, the state (7) is transparent for the two driving lasers (electromagnetically induced transparency, EIT). In this fashion an ideal dark state is prepared by phase-stable laser fields.

In the absence of dephasing the dark state (7) retains the phase relationship $\phi_0$ even when the atoms are suddenly shielded from the two laser fields for some time. Thus when the atoms are again exposed to the laser fields after this time, they still appear *dark*. However any phase difference $\Delta\phi_S$ acquired by the superposition state during the *laser-off* time results in a change of the absorption signal. Equally a phase change $\Delta\phi_L$ accumulated in the laser fields during the *laser-off* time will lead to a change of the absorption signal.

After a *laser-off* time of duration $T$ we have for equal Rabi frequencies and with $\Delta\phi_L - \Delta\phi_S = \Delta\phi$

$$|\langle 3|H_{\text{int}}|\psi_{\text{NC}}(T)\rangle|^2 = g^2[1 - \cos(\Delta\phi)]. \tag{11}$$

Since

$$|\langle 3|H_{\text{int}}|1\rangle|^2 = |\langle 3|H_{\text{int}}|2\rangle|^2 = g^2 \tag{12}$$

we see that the absorption of the superposition state rises to twice this value in the case of phase difference $\Delta\phi = \pi$, and is equal to $g^2$ for a phase difference $\Delta\phi = \pi/2$.

The additivity of phases in the observable (11) permits us to determine the signed value of a phase shift $\Delta\phi_S$ imprinted in the superposition state by comparison with a controlled phase shift $\Delta\phi_L$. The observable (11) can be cast into a dimensionless parameter which we termed brightness [17]. The dark-state absorption level is assigned a brightness of 0 whereas the incoherent mixture of observables (12) is assigned a brightness of 1. As discussed in [17], the brightness is a function of the relative phase between the laser fields and the phase appearing in the superposition state,

$$b(\Delta\phi) = 2\sin^2\left(\frac{\Delta\phi}{2}\right) \tag{13}$$

with $b(\Delta\phi) \in [0,2]$.

### A. Atomic Hamiltonian

The first-order perturbation energy (1) is a valid description of Zeeman energies at low magnetic field values. Nevertheless at kHz resolution higher-order corrections appear in the two-photon ground-state transition energy $|1\rangle \leftrightarrow |2\rangle$ due to the magnetic field Hamiltonian

$$\mathcal{H} = \frac{\mu_B}{\hbar}(g_S \vec{S} \cdot \vec{B} + g_I \vec{I} \cdot \vec{B} + \mathcal{A}\vec{S} \cdot \vec{I}), \tag{14}$$

as apparent from Fig. 3. Here $g_S$ and $g_I$ are the electron and nuclear spin $g$ values, $\vec{S}$ and $\vec{I}$ represent the valence electron spin and the nuclear spin respectively, and $\mathcal{A}$ is the Fermi-contact term where $\omega_{\text{hf}} = 2\mathcal{A}$.
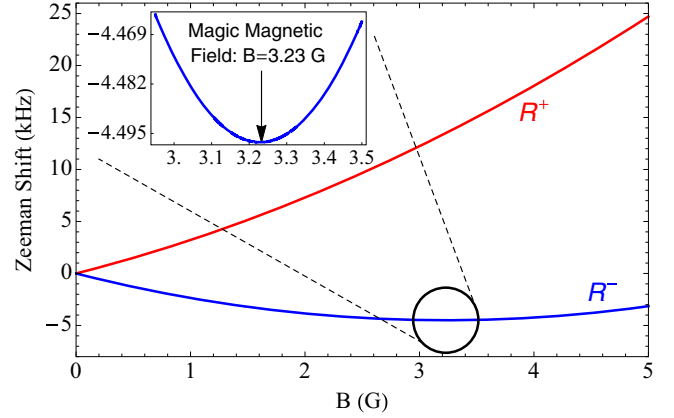


FIG. 3. (Color online) Zeeman shift of the $R^+$ and $R^-$ resonance in an external magnetic field. The zero-energy value is referenced to the hyperfine splitting $2\mathcal{A}$. Near $B = 3.23\,\text{G}$ the $R^-$ resonance is insensitive to small variations in $B$.

While it appears reasonable to use the first-order perturbation expression (1) for estimating the magnitude of the Berry phase we explored the effect of the full Hamiltonian (14) in calculating this phase. Using MATHEMATICA we were able to show that inserting (14) into (4) gives for the field strength $\vec{V}_\psi(\vec{B}) = m_F/B^2 \, \hat{e}_B$ with $\hat{e}_B$ the unit vector in the direction of $\vec{B}$ and the quantum number $m_F = m_S + m_I$. Hence the exact result for (2) can be written in the form of (5) despite the fact that the energy expression which appears in the denominator of (4) now contains terms nonlinear in both $g_S$ and $g_I$.

### B. Superposition state in a rotating magnetic field

Under rotation of the external magnetic field the two components of the superposition state acquire geometric phases $\gamma_1$ and $\gamma_2$, leaving the superposition state as

$$|\psi\rangle = (e^{i\gamma_1}|1\rangle - e^{i\gamma_2}e^{-i\phi_0}|2\rangle)/\sqrt{2}$$
$$= e^{i\gamma_1}(|1\rangle - e^{i\Delta\gamma}e^{-i\phi_0}|2\rangle)/\sqrt{2}. \tag{15}$$

Using Eq. (5) we obtain for the phase acquired after $n$ rotations of the magnetic field vector,

$$\Delta\gamma = \gamma_2 - \gamma_1 = -(m_{F_2} - m_{F_1})\,\Omega(C)$$
$$= -\text{sgn}(\theta)\,n\,2\pi(m_{F_2} - m_{F_1})(1 - \cos\theta), \tag{16}$$

a measure sensitive to the *difference in $m_F$ values* and to the signed opening angle of the rotation cone. Opposite signs appear in the phase expression for the $R^+$ and $R^-$ resonances; for the definition (15) we have

$$\Delta\gamma_\pm = \pm\,\text{sgn}(\theta)\,n\,4\pi(1 - \cos\theta). \tag{17}$$

We see that superposition states must be built from Zeeman levels with nonzero difference of their $m_F$ quantum numbers in order to imprint an observable Berry phase difference. As $\text{sgn}(\theta)$ is defined by the sign of the scalar product $\hat{n} \cdot \vec{B}$, the absolute sign of the result (17) defines the difference in observable angular momentum $(m_{F_2} - m_{F_1})\hbar$ of the two states participating in (15). The relative phase $\Delta\gamma$ is only defined modulo $2\pi$. A reasonable boundary condition is to demand $\Delta\gamma(\theta = 0) = 0$.
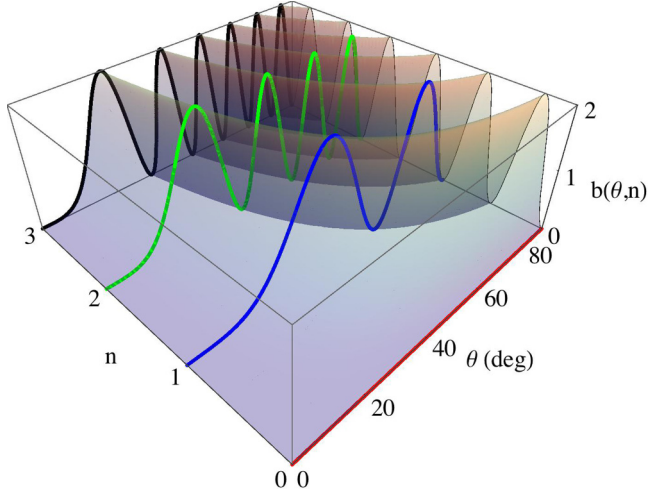
FIG. 4. (Color online) The Berry phase can be cast into the dimensionless observable brightness (18). The brightness measure is shown as a function of the cone angle $\theta$ and the number of rotations $n$.

The brightness measure is an experimental observable sensitive to the relative phase of the superposition state. Inserting for $\Delta\phi$ in Eq. (13) the value (17) we find a brightness measure depending on the cone angle

$$b(\theta,n) = 2\sin^2(\Delta\gamma/2)$$
$$= 2\sin^2(n\,2\pi(1-\cos\theta)), \quad (18)$$

which we show in Fig. 4 as a function of the number of rotations $n$. For one rotation ($n = 1$) $b$ oscillates twice between 0 and 2, maximally imprinting a phase of $4\pi$. For $n = 2$, the relative phase doubles resulting in $\Delta\gamma = 8\pi$ for $\theta = \pi/2$. A forward-backward rotation of the magnetic field compensates the geometric phase resulting in a brightness of 0 for an effective $n = 0$.

In the following we denote the time required in the experiment to rotate the magnetic field by $T$. The duration in our experiment is typically $T = 1$ ms. During this time (also termed as *laser-off* time) we turn off the external laser fields to isolate the phase evolution of the atomic state due to accumulation of geometric phase.

### C. Effect of decoherence

Our thermal superposition state suffers decoherence at a rate $\gamma_{\text{dec}}$ due to collisions and diffusion out of the laser interaction volume. For our setup the rate is typically $\gamma_{\text{dec}} = 2\pi \times 20$ Hz [18]. This gives rise to an additional phase change during the *laser-off* time $T$ due to buildup of an incoherent component in the ensemble. For large values of $T$ decoherence will saturate the brightness at $b = 1$. We take these effects into account using the model equation

$$b(\theta,T) = h(T) + 2[1-h(T)]\sin^2(\Delta\gamma/2), \quad (19)$$

where the buildup of the incoherent component scales as

$$h(T) = 1 - \exp(-\gamma_{\text{dec}}T). \quad (20)$$

### D. Dynamic phase

A dynamic phase will appear in case that the magnitude $|\vec{B}|$ is not kept constant during the *laser-off* time. Starting with an eigenstate $|\psi\rangle$ at time $t = 0$ and changing $|\vec{B}|$ in the time interval $(0,T)$ adiabatically, the final state is given by [1]

$$|\psi(T)\rangle = e^{-\frac{i}{\hbar}\int_0^T E_\psi(\vec{B}(t))dt}|\psi(0)\rangle. \quad (21)$$

Keeping $|\vec{B}|$ and therefore $E_\psi$ constant over time, the dynamic phase $e^{-iE_\psi T/\hbar}$ emerges. Note that now and from here onwards $E_n$ refers to the eigenvalues of the Hamiltonian (14) and not the first-order perturbation result (1). To stabilize the dynamic phase from fluctuating magnetic fields we carry out most experiments with the $R^-$ resonance at $|\vec{B}| = 3.23$ G at which magnetic field value the state energy difference is insensitive to small variations of the field; see Fig. 3.

In the absence of the laser fields and with $|\vec{B}|$ constant the dark state propagates with the relative dynamic phase $(E_2 - E_1)T/\hbar$. Under ideal conditions this phase evolution matches that of the laser fields $(\omega_2 - \omega_1)T$.

### E. ac-Stark shift

When the laser fields are on, the position of the $R^-$ resonance is affected by a small ac- Stark shift $\omega_{\text{ac}}$. Thus with the lasers on we have the dark-state condition

$$(E_2 - E_1)/\hbar + \omega_{\text{ac}} = \omega_2 - \omega_1. \quad (22)$$

As a result when the atoms are kept in the dark for a time $T$, atoms and laser fields get out of tune by

$$\phi_{\text{ac}} = \omega_{\text{ac}}T. \quad (23)$$

We measured [18] the ac-Stark shift for the $R^-$ resonance to be positive $\omega_{\text{ac}}/I \approx +2\pi \times 0.15\,\frac{\text{Hz}}{\mu\text{W/cm}^2}$, where $I$ is the sum of both laser intensities. During the dark period the ac-Stark effect gives rise to the additional phase offset $\phi_{\text{ac}} = \omega_{\text{ac}}T$, which modifies Eq. (19) for the brightness to

$$b(\theta,T) = h(T) + 2[1-h(T)]\sin^2\left(\frac{\Delta\gamma}{2} + \frac{\omega_{\text{ac}}T}{2}\right). \quad (24)$$

In Eq. (24) the absolute sign of $\Delta\gamma$ is accessible in relation to a known value $\omega_{\text{ac}}T$. Unless otherwise noted all measurements are carried out at laser intensities below 75 $\mu$W/cm$^2$. For $T = 1$ ms we then accumulate $\phi_{\text{ac}} \leqslant +4°$, a level just below our detection limit.

### F. Effect of detuning from EIT resonance

Equation (18) holds for zero detuning from EIT resonance. A generalization of the brightness measure for a a small two-photon detuning $\delta$ was given in [17] in the limit $\Gamma > \delta$ and $g^2/\Gamma \gg \gamma_{\text{dec}}$, where $\Gamma$ is the decay rate of the excited state $|3\rangle$. Accounting for the detuning we rewrite (18) as

$$b(\theta,\delta,T) = h(T) + (1-h(T))$$
$$\times\left[2\sin^2\left(\frac{\Delta\gamma + \delta T}{2}\right) + \mathcal{G}\sin(\Delta\gamma + \delta T)\right]$$
$$= h(T) + (1-h(T))$$
$$\times[1 + \sqrt{1+\mathcal{G}^2}\sin(\Delta\gamma + \phi_d - \pi/2)] \quad (25)$$

where we neglected the ac-Stark induced phase shift and we used the abbreviations

$$\phi_d = +\delta T - \arctan\frac{1}{\mathcal{G}} + \pi/2, \qquad (26)$$

$$\mathcal{G} = \Gamma\delta/(g^2 - \delta^2). \qquad (27)$$

Note that the brightness defined by Eq. (25) can exceed the value of 2. Also in Eq. (25) the absolute sign of $\Delta\gamma$ is accessible, now in relation to a known value, $\delta T$. The definition of the detuning we use is

$$\delta = \omega_2 - \omega_1 - \omega_{hf}. \qquad (28)$$

### G. Phase shift in free-induction decay

A third method exists which is sensitive to the sign of the geometric phase and covers its magnitude modulo $2\pi$. Here we prepare the dark state at two-photon resonance, but deliberately detune the lasers by $\delta$ at the end of the *laser-off* time ($t = 0$). Now damped Rabi oscillations of the free-induction decay of the absorption signal reveal the phase of the superposition state. The free-induction decay (Eq. (24) in [18]) gives rise to a brightness

$$b(t,\delta) \propto 1 - \cos(\delta t + \Delta\gamma)e^{-\Gamma' t}, \qquad (29)$$

where $\Gamma' = g^2/\Gamma \gg \gamma_{dec}$, a condition always met in our experiment.

### IV. EXPERIMENT

Figure 5 shows schematically our experimental setup. We use $^{87}$Rb atoms in a 75 mm long quartz cell at 25 °C. The cell contains neon buffer gas at a pressure of 20 torr. We employ two external cavity diode lasers. A master laser is locked on the $^2S_{1/2} \leftrightarrow {}^2P_{1/2}$ transition. An optical phase-locked loop (OPLL) phase-stabilizes a slave laser against this master laser. The two phase-stabilized laser fields are then coupled into an optical fiber. They are expanded to a diameter of $\approx 15$ mm at which they propagate through the Rb cell before being focused on a photodiode for detection of an absorption signal.

The Rb cell is located in a cylindrical magnetic field coil of length 30 cm. This coil is used for the quantization field along the $z$ direction, providing a constant field, $B_z = 3.23$ G. A twin coil is used to correct the $z$ field during rotation in order to keep $|\vec{B}|$ constant while rotating the $\vec{B}$ field vector. Rotation is achieved by applying magnetic fields along the $x$ and the $y$ directions using two pairs of rectangular Helmholtz coils ($35 \times 226$ mm). We generate single cycles of sine and of cosine shape using two waveform generators (Syscomp WGM 201). Their signals are fed into audio amplifiers (System Fidelity SA-300 SE) to generate the transverse field components. In order to keep the absolute value of $\vec{B}$ constant, the $B_z$ component is decreased by applying an appropriate time- and $\theta$-dependent current to the twin coil. Since the magnetic field vector points initially along the $z$ direction, the magnetic field vector is first tilted by an angle $\theta$ relative to the $z$ axis, then rotated before being aligned in the $z$ direction again. It takes $\approx 30 \,\mu$s to tilt the magnetic field vector. Prior to transport of the magnetic field vector both laser beams are blocked from entering the Rb cell.
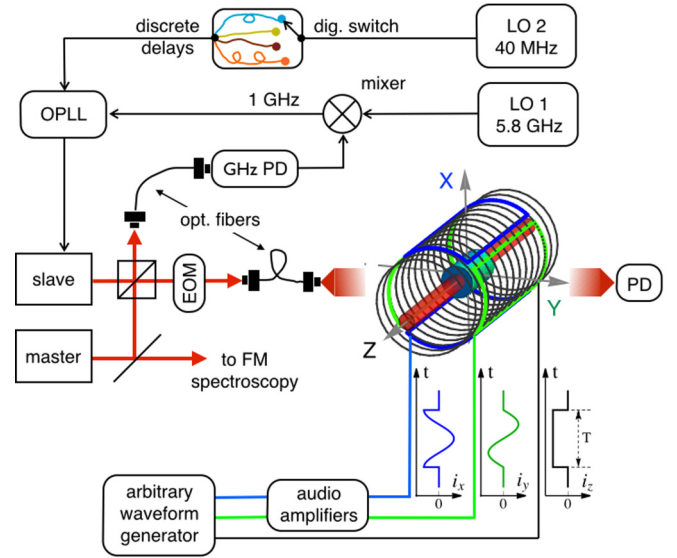


FIG. 5. (Color online) Experimental setup. A slave laser is stabilized to a master laser via an optical phase-locked loop (OPLL). The laser beat signal is mixed with the signal from the local oscillator LO1 to a difference frequency near 1 GHz. The OPLL compares this signal with that from a second oscillator LO2. Its frequency can be tuned and its phase can be changed by choosing discrete delay lines. The expanded laser beams propagate through the cell before being detected on a photodiode (PD). Six field coils allow temporal control of the magnetic field vector. During the time $T$ when the field is rotated the lasers are blocked with an electro-optic modulator (EOM).

The error on the $\theta$ value is evaluated by measuring the current of the four coils with a current probe (Agilent N2782B). At each point in time during $T$ (in steps of 2 $\mu$s) we calculate the current angle from the four probe currents. The deviation from the mean of these values is representative for the error in $\theta$ for which we found the relationship $\Delta\theta = 0.23(1 + \theta/10)$ where $\theta$ is given in degrees. At $|\vec{B}| = 3.23$ G, the $m_F = \pm 1$ states have Larmor frequencies $\omega_L = \mp 2\pi \times 2.26$ MHz, much larger than the typical magnetic field rotation frequency used (1 to 10 kHz).

After the time span $T$ during which the magnetic field is rotated, the laser beams are transmitted again and phase changes imprinted in the ensemble result in a rise of the absorption signal. A typical measurement cycle to obtain the Berry phase entails the sequence of events shown in Fig. 6. This trace is the sum of 100 scans. It is obtained after subtracting an equivalent measurement at a large detuning from resonance. This compensates a minor transmission overshoot in the photodiode signal when switching the EOM at the end of the *laser-off* time.

The sequence in Fig. 6 begins with the preparation of $|\psi_{NC}\rangle$ at times prior to the *laser-off* time $T$. After turning on the lasers again at $t = 0$ a rise of the absorption signal is observed, dependent upon the phase changes incurred during the dark period $T$. Following the turn-on of the lasers, an exponential return into the dark state ensues [18]. At late times, when EIT conditions are again reached, three consecutive phase jumps are applied to reference the absolute scale for the phase change.
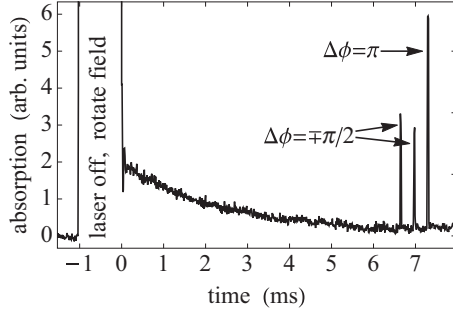
FIG. 6. The dark state is prepared at times $t < -1$ ms. Both lasers are then turned off with the EOM and turned on again at $t = 0$. Any phase change of the superposition state is reflected by a rise in the absorption signal. This signal decays exponentially back into the dark state for $t > 0$. At late times three phase jumps of 30 $\mu$s duration are performed, $\mp\pi/2$, $\pm\pi/2$, and $\pm\pi$, to calibrate the brightness scale.

Two consecutive phase jumps of $-\pi/2$ at 6.6 ms followed by $+\pi/2$ 30 $\mu$s later and of $+\pi/2$ at 6.9 ms followed by $-\pi/2$ serve to check two-photon resonance. Resonance is signified [17] by equal height of the two absorption signals. The associated changes in absorption reference the brightness measure $b = 1$. A third phase jump by $\pi$ (at 7.2 $\mu$s in Fig. 6) sets the scale $b = 2$.

The phase jumps are realized by switching the reference signal to the OPLL between cables of appropriate length, the box marked discrete delays in Fig. 5. The digital switch to cables of different length (Minicircuits ZSWA-4-30 DR) is controlled by a sequence of TTL pulses generated by a pattern generator (Syscomp WGM 201). With this method, we can determine the two-photon resonance position to $\pm3$ Hz and phase changes at a level of precision of typically $\pm5°$.

When operating on two-photon resonance the method in Fig. 6 yields a brightness measure (19) which carries no information on the absolute sign of the geometric phase. However, when operating at a small detuning from two-photon resonance (24) or in the presence of a significant ac-Stark shift of known sign (25), a reference appears which allows us to determine its absolute sign.

We also have access to the sign by deliberate detuning of the laser fields to a position far from resonance ($\delta > \Gamma$), just prior to monitoring absorption at the end of the *laser-off* time. In this situation Ramsey interference fringes appear in the free-induction decay of the superposition state. A typical measurement sequence using this method is shown in Fig. 7. Here the slave laser is detuned by $\delta = 2\pi \times 2$ kHz at the end of the *laser-off* time. As predicted by Eq. (29) Rabi-oscillations at frequency of 2 kHz are observed in the free-induction decay between $t = 0$ and $t = 1.8$ ms. At the latter time the lasers are tuned back to two-photon resonance again. The Berry phase derives from a comparison of the phase of oscillations with and without rotation of the magnetic field as discussed in the caption to Fig. 7.

## V. RESULTS

Figures 8(a) and 8(b) show experimental data for the brightness as a function of the cone angle $\theta$ for $n = 1$ and $n = 2$
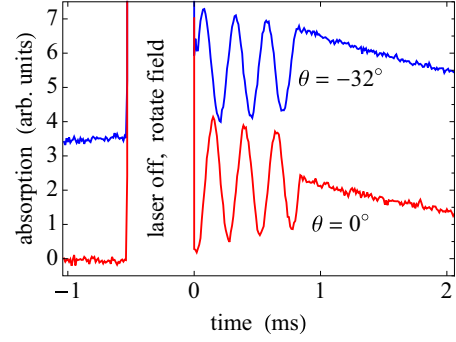


FIG. 7. (Color online) Rabi oscillations appear in the free-induction decay ($t > 0$) when using lasers detuned by $\delta = +2\pi \times 2$ kHz from two-photon resonance. For the blue curve the cone angle was $\theta = -32°$, for the red curve we had $\theta = 0°$. Fitting Eq. (29) to the oscillatory signals yields a phase shift difference $\phi_s(-32°) - \phi_s(0°) = \Delta\gamma = 105.4 \pm 0.4°$. Equation (16) predicts a Berry phase $\Delta\gamma = +109°$ for $\theta = -32°$. On the other hand $\Delta\gamma = +105.4°$ is predicted for $\theta = -31.4°$, a value commensurate with the precision at which we can control $\theta$.

rotations for a *laser-off* time of $T = 1$ ms at $|\vec{B}| = 3.23$ G. Good agreement of the experimental data with the predictions of Eq. (19) is found. The offset from brightness $b = 0$ and $b = 2$ is due to the decoherence rate $\gamma_{\text{dec}}$ which enters the expression $h(T)$. In all measurements the fits revealed decoherence rates
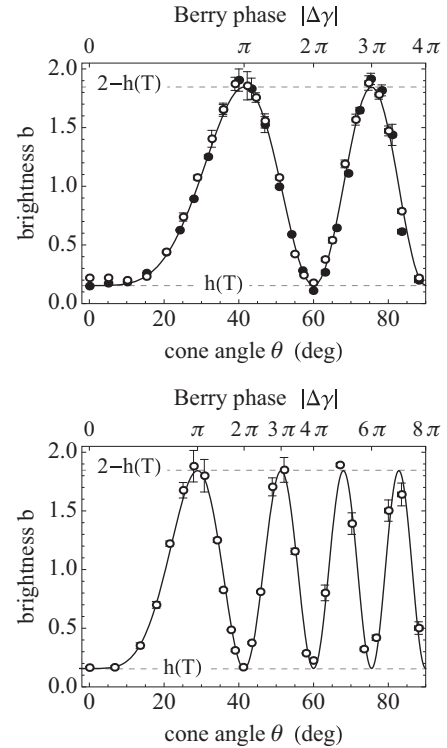


FIG. 8. Brightness as a function of the cone angle $\theta$ for $n = 1$ (top) with a rotation frequency of $f_{\vec{B}} = 1$ kHz is shown as full circles in the top figure. Open circles are data recorded at $f_{\vec{B}} = 10$ kHz. The bottom figure gives data for $n = 2$ rotations recorded at $f_{\vec{B}} = 2$ kHz. Full curves represent fits of Eq. (19).
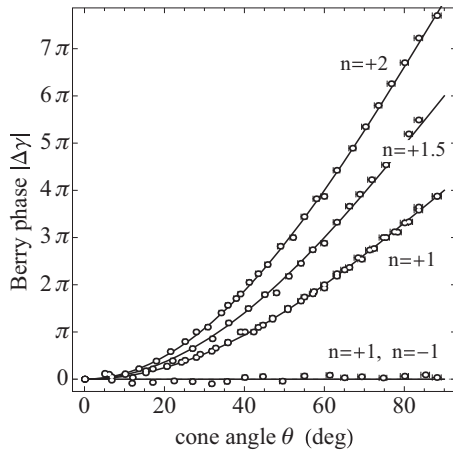
FIG. 9. The absolute value of the Berry phase for $n = 1$, 1.5, and 2 rotations as a function of the cone angle $\theta$. Also shown is the case when the magnetic field vector circumscribes the spherical circuit and then returns on the same path, giving an effective rotation $n = 0$.

$\gamma_{\text{dec}} = 2\pi \times (25 \pm 5)$ Hz. The measurements in Fig. 8 were recorded at a laser intensity of $I = 65\ \mu\text{W/cm}^2$. This low intensity leads to an ac-Stark phase of $\phi_{\text{ac}} \approx 3.5°$ which is not noticeable on the scale shown.

The geometric phase is independent of the rotational frequency of the magnetic field vector $f_{\vec{B}}$ as long as adiabaticity is assured. This property is verified experimentally in Fig. 8, top, where data recorded at a rotational frequency of $f_{\vec{B}} = 1$ and 10 kHz are compared.

Figure 9 collects values of the absolute value of the Berry phase as a function of the cone angle $\theta$ for $n = 1$ and 2. Also included is the case $n = 1.5$ where the magnetic field vector is rotated by 540° before being returned into the original position. Finally the result of an experiment is shown where the $z$ axis was once encircled in the positive and once in the negative direction along the same path ($n = +1$, $n = -1$). When the magnetic field vector circumscribes a spherical path and returns along the same path the effective rotation is $n = 0$ and the experiment testifies the dependence of Berry's absolute phase on the direction of rotation.

### A. Effect of ac-Stark shift

An ac-Stark effect of the eigenstates shifts the central frequency of the dark resonance and manifests itself as a buildup of a phase shift $\phi_{\text{ac}}$ during the *laser-off* time. At higher laser intensities this effect can be prominent and we can model the situation using Eq. (24). Figure 10 compares a measurement at a laser intensity of $I = 237\ \mu\text{W/cm}^2$ with that at low intensity. For the data in Fig. 10, the magnetic field was rotated clockwise as well as anticlockwise. We see that at low intensity a practically symmetric pattern emerges while the oscillations shift to larger cone angles when the laser intensity is high. As predicted by Eq. (24) the oscillations in brightness due to the Berry phase are shifted along the $\theta$ coordinate due to the positive sign of $\phi_{\text{ac}}$. Equation (23) predicts $\phi_{\text{ac}} = 12.8°$, in agreement with the experimental fit of the data in Fig. 11 (full line) of $13.5° \pm 0.6°$. We expect that a Berry phase shift by $-13.5°$ should balance the ac-Stark
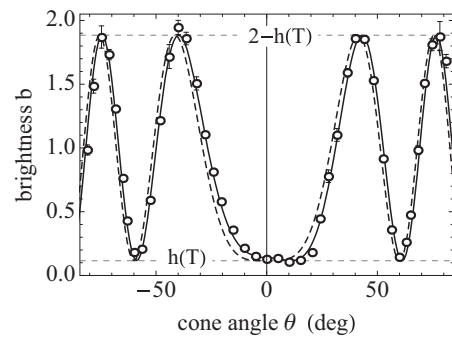


FIG. 10. The brightness as a function of the cone angle $\theta$ for $n = 1$ recorded at an intensity of $I = 237\ \mu\text{W/cm}^2$ shows the effect of a significant ac-Stark phase. The dashed curve represents a fit to data recorded at $I = 65\ \mu\text{W/cm}^2$. The sign of the cone angle indicates the direction of rotation around the laboratory $z$-axis, see discussion after Eq. (6).

induced shift of the phase. This is indeed observed at $\theta_c \approx 11°$, the apparent center position of the oscillations in Fig. 10, at which $4\pi(1 - \cos\theta_c) \approx 13.5°$. We note that this observation proves the sign of geometric phase as predicted by (17). For the $R^-$ resonance a negative geometric phase appears for positive rotation angle $\theta$.

### B. Effect of detuning from resonance

A second situation where the geometric phase appears in relation to a known reference is when the laser frequencies are permanently at some small two-photon detuning $\delta$ from resonance. A fringe shift is observed, accompanied by the appearance of an asymmetry, as shown in Fig. 12. Here we compare the brightness response for the $R^-$ resonance (top) with the result for the $R^+$ resonance (bottom figure) under otherwise identical conditions, a detuning from resonance by $\delta = +2\pi \times 30$ Hz. From (17) one expects the Berry phase for the two resonances to have opposite sign. This is reflected by the opposing asymmetry found for the two resonances with respect to the direction of rotation. According to Eq. (25) a positive detuning $\delta$ requires a negative geometric phase to counterbalance the contribution $\phi_d$. This occurs at $\theta \approx +20°$ for $R^-$ and at $\theta \approx -20°$ for $R^+$ when the two states show
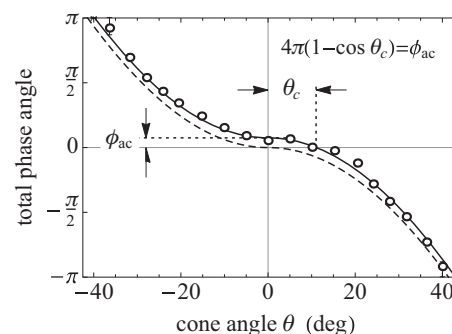


FIG. 11. The total phase extracted from the data in Fig. 10 reveal the presence of the ac-Stark phase $\phi_{\text{ac}}$. The dashed line shows the geometric phase $\Delta\gamma$, obtained after subtracting $\phi_{\text{ac}}$ from the measured total phase values.
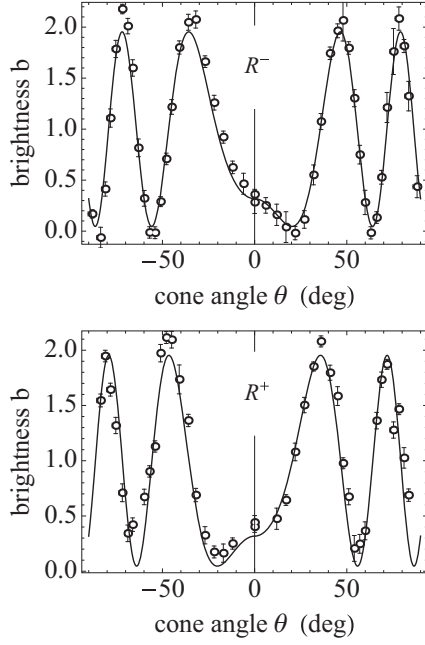
FIG. 12. Brightness as a function of the cone angle $\theta$ for $n = 1$, $f_{\tilde{B}} = 1$ kHz for the $R^-$ resonance (top) and the $R^+$ resonance (bottom). The two-photon detuning was $\delta = +2\pi \times 30$ Hz. The full curves show the common fit to both data sets using Eq. (25), yielding the fit parameter $|\mathcal{G}| = 0.98 \pm 0.05$. Hence (27) implies $g^2/(\delta\Gamma) \approx 1$. With $\Gamma = 2\pi \times (190 \pm 30)$ MHz we find from this fit $g \approx 2\pi \times (75 \pm 12)$ kHz, in agreement with the value expected at $I = 65\ \mu\text{W/cm}^2$.

minimal brightness. Equivalent experiments carried out at a negative detuning (not shown) confirmed the change of sign of rotation for balancing phases.

The total phase extracted from the data in Fig. 12 as a function of $\theta$ is collected in Fig. 13. Here we see the Berry phase accumulated for the two resonances in relation to the known phase $\phi_d$ which is generated by the +30 Hz detuning. Using our pressure broadened value $\Gamma = 2\pi \times (190 \pm 30)$
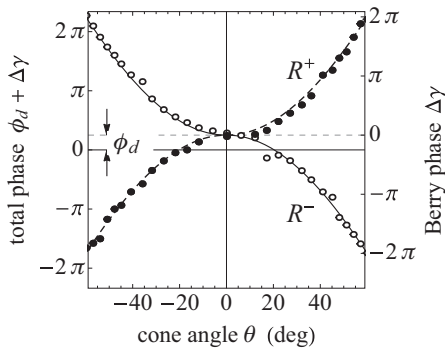


FIG. 13. The total phase accumulated when the lasers are operated 30 Hz detuned from two-photon resonance is shown by the open ($R^-$) and filled ($R^+$) circles respectively. Without rotating the magnetic field the +30 Hz detuning gives rise to a phase shift $\phi_d \approx 0.26\,\pi$. When rotating the magnetic field the $R^-$ and $R^+$ resonances reveal the opposite sign of their Berry phase which is offset by the identical phase shift $\phi_d$.
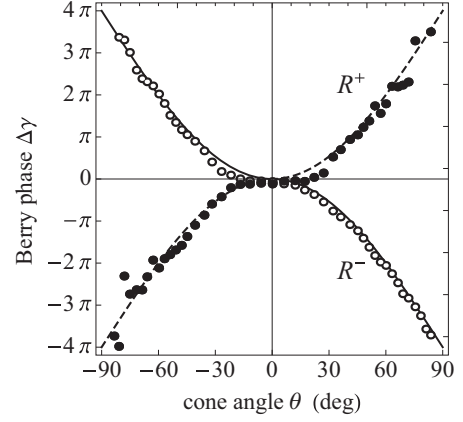


FIG. 14. Berry phase as function of the cone angle extracted from the phase shifted oscillations in free-induction decay. The solid and dashed lines give the prediction (16).

MHz [19] we estimate from Eq. (25) the Rabi frequency $g = 2\pi \times 75$ kHz, a value quite consistent [18] with the laser intensity used, $I = 65\ \mu\text{W/cm}^2$.

The observed direction of asymmetry for $R^+$ and $R^-$ again confirms the absolute sign of the geometric phase given in Eq. (17), consistent with its independence of $g_F$.

### C. Berry phase in free-induction decay

A third alternative for direct access to the geometric phase is to operate on two-photon resonance but to probe the absorption signal at the end of the laser-off time with a detuned laser field; see Fig. 7. A collection of data recorded by this method is given in Fig. 14. When plotting the phase difference accumulated with and without rotation this method gives the geometric phase modulo $2\pi$ inclusive of its sign. Again the mirror symmetry of the sign of the Berry phase for the two resonances and their sign relative to the sign of the rotation angle reveals the independence of the geometric phase from the Landé factor. It may be observed that the precision of data recorded for the $R^-$ resonance is superior to that for $R^+$. The reason for this is understood in the context of Fig. 3. The steep slope of the energy dependence of the $R^+$ resonance on magnetic field leads to a much higher sensitivity to magnetic field fluctuations and hence small uncontrolled dynamic phase shifts.

### VI. CONCLUSION

We explore the ramifications of the Berry phase on dark superposition states of thermal $^{87}$Rb atoms. The Berry phase concerns a purely geometrical connection between the observable total angular momentum and a laboratory axis around which the total angular momentum vector is guided on an adiabatic path. We explore and confirm this relationship over a wide parameter range using dark-state atoms prepared by electromagnetically induced transparency using two phase-stable laser fields. These atoms are allowed to evolve in the absence of laser fields and accumulate a geometric phase from rotation of the laboratory magnetic field. This phase can be monitored with high sensitivity by interrogating the atoms with laser fields of controlled phase

relationship. The precise determination of the relative phase in the superposition state gives access to phase changes of dynamic and of geometric origin. The latter are studied as a function of the solid angle of circuits of a rotating laboratory magnetic field. Six computer-controlled field coils made it possible to vary the solid angle circumscribed by the magnetic field vector between 0 and $2\pi$ while keeping the magnitude $|\vec{B}|$ constant during the rotation.

We demonstrate that by reference to an experimentally controlled phase of known sign we have access to the absolute sign of the geometric phase. This we show at the example of an ac-Stark shift related phase and by choosing conditions deliberately detuned from atomic resonance. Important properties of the geometric phase were verified such as its independence of the rotational frequency $f_{\vec{B}}$, and its sign dependence on the direction of rotation of $\vec{B}$. Comparing the geometric phase for resonances involving Zeeman states of opposite $m_F$ quantum number but identical Landé factor we ascertain its independence of the sign of the Landé factor.

Our experiment also emphasizes the greater role played by the sign of the Berry phase for a Zeeman level $m_F$. Geometric rotation of a quantum state about the direction of the external $\vec{B}$ field enters the phase (5) along with the observable magnitude of total angular momentum $m_F\hbar$. The latter is generally assigned from the energy scale of a Zeeman spectrum knowing laser polarization or the Landé factor. A Berry phase experiment on the other hand reveals the purely geometric nature of space quantization of action. A positive sign of this phase indicates that the observable angular momentum vector is antiparallel to the axis of rotation $\hat{n}$ and to the quantization axis which lifts the degeneracy of angular momentum, irrespective of magnitude and sign of the energetic splitting.

[1] M. V. Berry, Proc. R. Soc. London Ser. A **392**, 45 (1984).

[2] G. Herzberg and H. C. Longuet-Higgins, Discuss. Faraday Soc. **35**, 77 (1963).

[3] H. C. Longuet-Higgins, Proc. R. Soc. London Ser. A **344**, 147 (1975).

[4] Y. Aharanov and L. Susskind, Phys. Rev. **158**, 1237 (1967).

[5] A. Tomita and R. Y. Chiao, Phys. Rev. Lett. **57**, 937 (1986).

[6] T. Bitter and D. Dubbers, Phys. Rev. Lett. **59**, 251 (1987).

[7] R. Tycko, Phys. Rev. Lett. **58**, 2281 (1987).

[8] C. L. Webb, R. M. Godun, G. S. Summy, M. K. Oberthaler, P. D. Featonby, C. J. Foot, and K. Burnett, Phys. Rev. A **60**, R1783 (1999).

[9] P. J. Leek et al., Science **318**, 1889 (2007).

[10] S. Filipp, J. Klepp, Y. Hasegawa, C. Plonka-Spehr, U. Schmidt, P. Geltenbort, and H. Rauch, Phys. Rev. Lett. **102**, 030404 (2009).

[11] A. Morinaga, T. Aoki, and M. Yasuhara, Phys. Rev. A **71**, 054101 (2005).

[12] A. Morinaga, K. Toriyama, H. Narui, T. Aoki, and H. Imai, Phys. Rev. A **83**, 052109 (2011).

[13] A. Morinaga and K. Nanri, Phys. Rev. A **86**, 022105 (2012).

[14] D. J. Richardson, A. I. Kilvington, K. Green, and S. K. Lamoreaux, Phys. Rev. Lett. **61**, 2030 (1988).

[15] J. J. Sakurai, in *Modern Quantum Mechanics, Revised Edition*, edited by S. F. Tuan (Addison-Wesley, New York, 1994).

[16] Y. Aharonov and J. Anandan, Phys. Rev. Lett. **58**, 1593 (1987).

[17] C. Basler, K. Reininger, F. Meinert, P. N. Ghosh, and H. Helm, Phys. Rev. A **87**, 013430 (2013).

[18] F. Meinert, C. Basler, A. Lambrecht, S. Welte, and H. Helm, Phys. Rev. A **85**, 013820 (2012).

[19] D. A. Steck, rubidium 87 D line data, University of Oregon, 2010, http://george.ph.utexas.edu/~dsteck/alkalidata/rubidium87numbers.pdf.